Electronic Supplementary Material (ESI) for RSC Advances.
This journal is © The Royal Society of Chemistry 2014

Supplementary Information

Sub-diffraction imaging of nitrogen-vacancy centers in diamond by stimulated emission depletion and structured illumination

Xusan Yang[†a],Yan-Kai Tzeng[†b], Zhouyang Zhu[c], Zhihong Huang[d], Xuanze Chen[a], Yujia Liu[a], Huan-Cheng Chang[c], Lei Huang[e*], Wen-Di Li[c*], Peng Xi[a*]

[a] *Department of Biomedical Engineering, College of Engineering, Peking University,No.5,Rd Yiheyuan, Beijing, China.*
[b]*Institute of Atomic and Molecular Sciences, Academia Sinica, Taipei, Taiwan*
[c]*Department of Mechanical Engineering, University of Hong Kong, Hong Kong, China. E-mail: liwd@hku.hk*
[d]*Intelligent Infrastructure Lab, Hewlett-Packard Labs, Palo Alto, USA*
[e] *Center of Biomedical Analysis, Tsinghua University, Beijing, China*
[*] *Corresponding authors: xipeng@pku.edu.cn liwd@hku.hk lhuang@center.biomed.tsinghua.edu.cn*
[†]*These authors contribute equally to this study*

1. TEM image of the FND nanoparticles

The FND nanoparticles were imaged with transmission electron microscope (H9000, Hitachi, Japan). Since the FND nanoparticles show irregular shape and aspect ratio (Supplementary Figure 1a), the diameters of the short axis are measured and statistically analyzed (Supplementary Figure 1b). The average size of the FNDs is 34.3±4.2 nm.

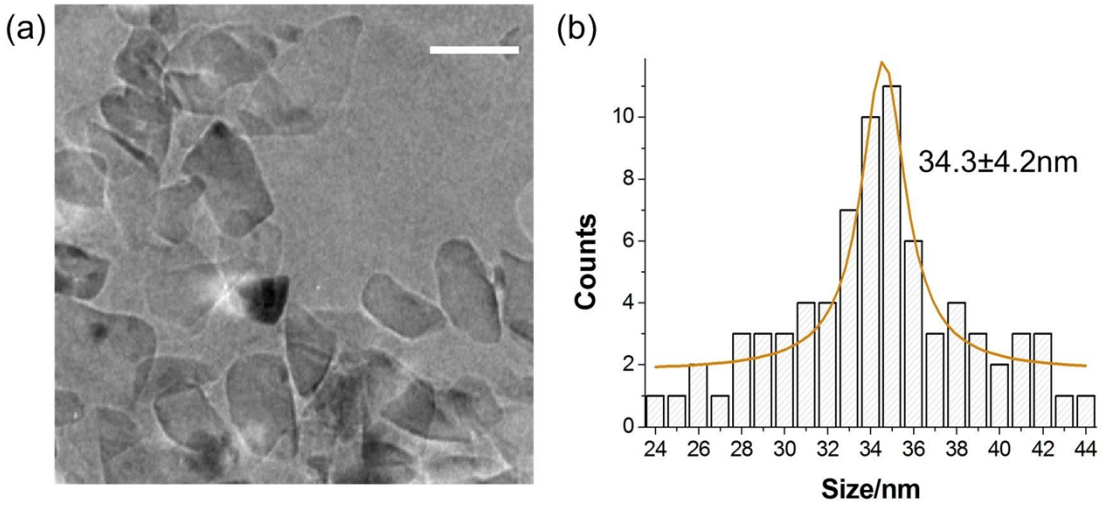

Supplementary Figure 1 TEM imaging of FND particles（a）and their size distribution (b). Scale bar, 50 nm.

As the resolution is calculated with subtraction of the particle size in two-dimension: $d_{resolution} = \sqrt{d_{FWHM}^2 - d_{size}^2}$, the conservative estimation of the nanoparticle

size can lead to an under-estimation of the resolution enhancement, especially when the resolution is comparable to the particle size.

2. Emission spectra of the FND nanoparticles and NV centers in bulk diamond

The excitation spectrum of the 35nm FND was acquired by using an inverted microscope (TCS SP8, Leica, Germany) equipped with a pulsed white light laser system with wavelength of 470~670nm and repetition rate of 78 MHz. The FND was fixed on the coverslip glass by spin coating for optimal spectrum measurement. The excited light was chosen from 470 to 650 nm, and the resolution wavelength is 1 nm. Fluorescence was collected through an oil-immersion objective (63x, NA 1.4) and detected with a GaAsP hybrid detection system at the emission band of 700~800nm. To avoid the background interference, the detection was time-gated from 4 to 12ns.

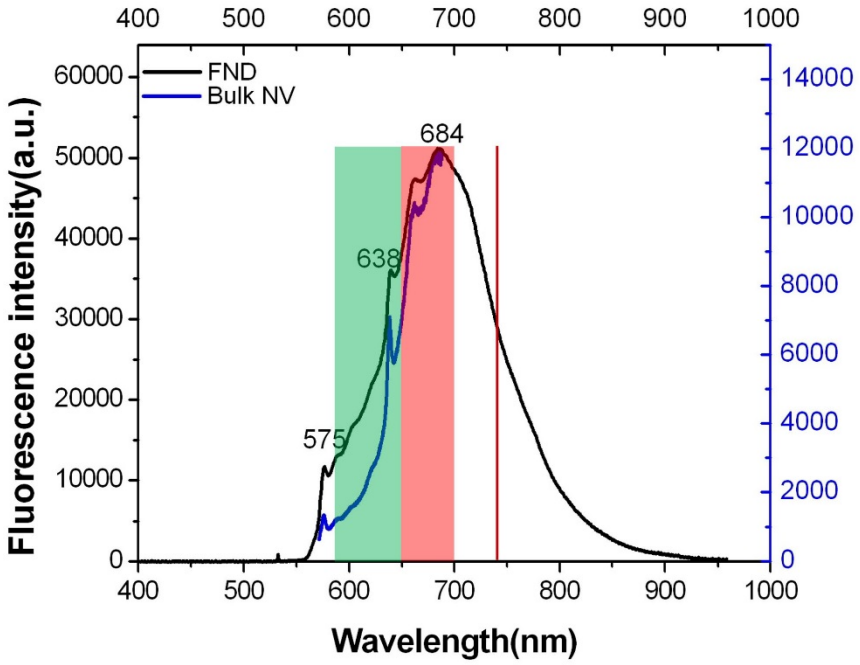

Supplementary Figure 2 Fluorescence spectra of NV center in the fluorescent nanodiamond particle solution (black) and NV dot array patterns (blue) on the bulk diamond. The green region is the fluorescent collection window of 592-650nm (Semrock, USA) for SIM. The red region and red line denotes the fluorescence collection window of 650-700nm and donut wavelength of 743 nm for STED.

Emission spectra of FNDs suspended in water were acquired by using a home-built setup in Taiwan, which consists a continuous-wave 532 nm laser (DPGL-2100F, Photop Suwtech), a dichroic mirror (Z532RDC, Chroma), a long-working distance microscope objective (50x, NA 0.55, Mitutoyo), a long-pass edge filter (E550LP, Chroma), and a multichannel analyzer (C7473, Hamamatsu), as previously described

(Y.-R. Chang, et al. *Nature Nanotech.* **3**, 284–288 (2008)). Fluorescence was collected in a backward geometry to prevent strong light scattering loss due to the high refractive index of the FND nanoparticles. The photoluminescence emission spectrum of the NV centers created by focused helium ion beam implantation on the bulk diamond was characterized using a home-built confocal microscope setup in Hewlett-Packard Labs. A 532 nm laser was used to excite the NV centers at room temperature. As NV centers are embedded in the diamond matrix, FND particles from these two sources show essentially the same spectra (Supplementary Figure 2), although the spectrometric measurement of the bulk NV center is limited to 690nm. The sharp peaks at 575 nm and 638 nm correspond to the zero-phonon lines of neutral and negatively charged NV centers (NV^0 and NV^-), respectively.

3. Artifact of SIM associated with axial focal displacement

Comparing to conventional wide field microscopy, SIM results (c and f) have a little axial shift which was caused by different wavefront of conventional wide field path and SIM optical path, due to the additional grating and other optical elements in SIM configuration. From (d) and (f), we can see that the three dots in the two images didn't match well (yellow dotted lines).The pseudo wide-field microscopy result (b and e) generated from the superposition of the 9 SIM frames matched well with the SIM microscopy result (c and f).

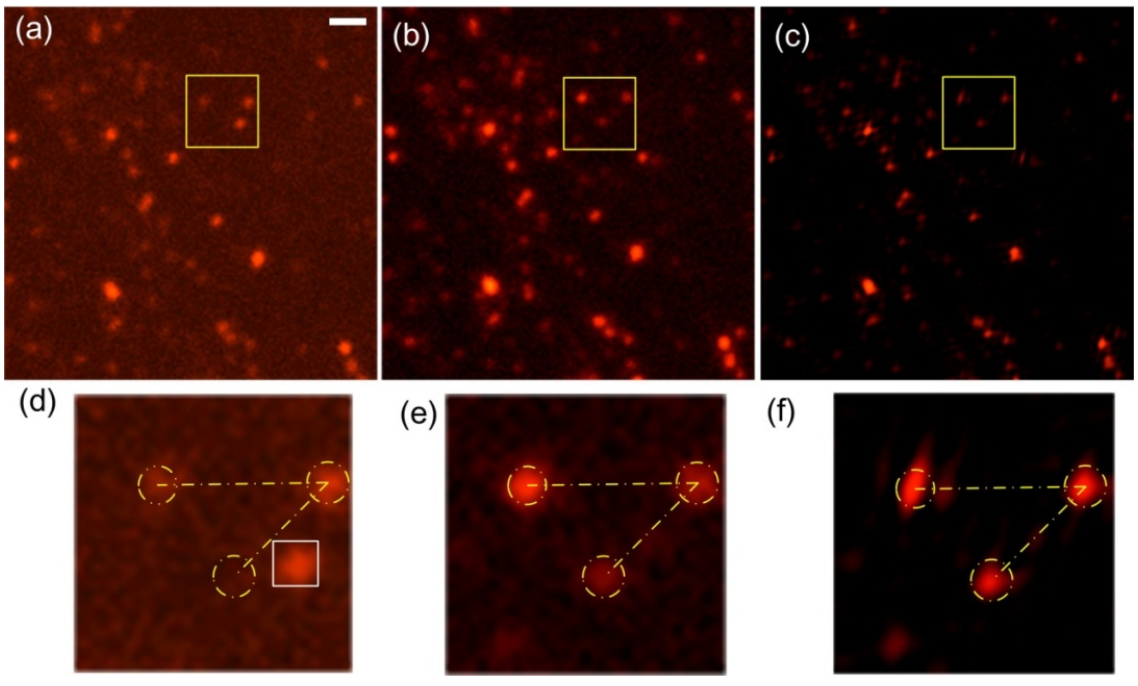

Supplementary Figure 3 Imaging of FNDs with conventionalwide-field (a and d), the pseudowide-field

microscopy (b and e) and SIM microscopy (c and f). Magnifications of the boxed areas (yellow) in (a), (b) and (c)were shown in view (d),(e)and (f), respectively. Pixel sizes of the wide-field and SIM microscopy are 60 nm and 30 nm, respectively, and the exposure time is 9 s for each frame. Scale bar, 1 μm.

4. Imaging of mouse kidney with SIM

To demonstrate the capability of our SIM system in biological specimen, a cryostat section of mouse kidney sample (Invitrogen, F24630) stained with Alexa Fluor 488 wheat germ agglutinin, Alexa Fluor 568 phalloidin, and DAPI was used. Alexa Fluor 488 wheat germ agglutinin was used to label elements of the glomeruli and convoluted tubules. Alexa Fluor 568 conjugated to phalloidin was utilized as fluorescent label of the filamentous actin in the brush boarder of the mouse kidney. As can be seen from Supplementary Figure 4 and 5, the resolution of SIM in both cases reaches ~140 nm in both cases, which is ~2-fold improvement over wide-field microscopy, enabling the visualization of the fine structures of the specimen.

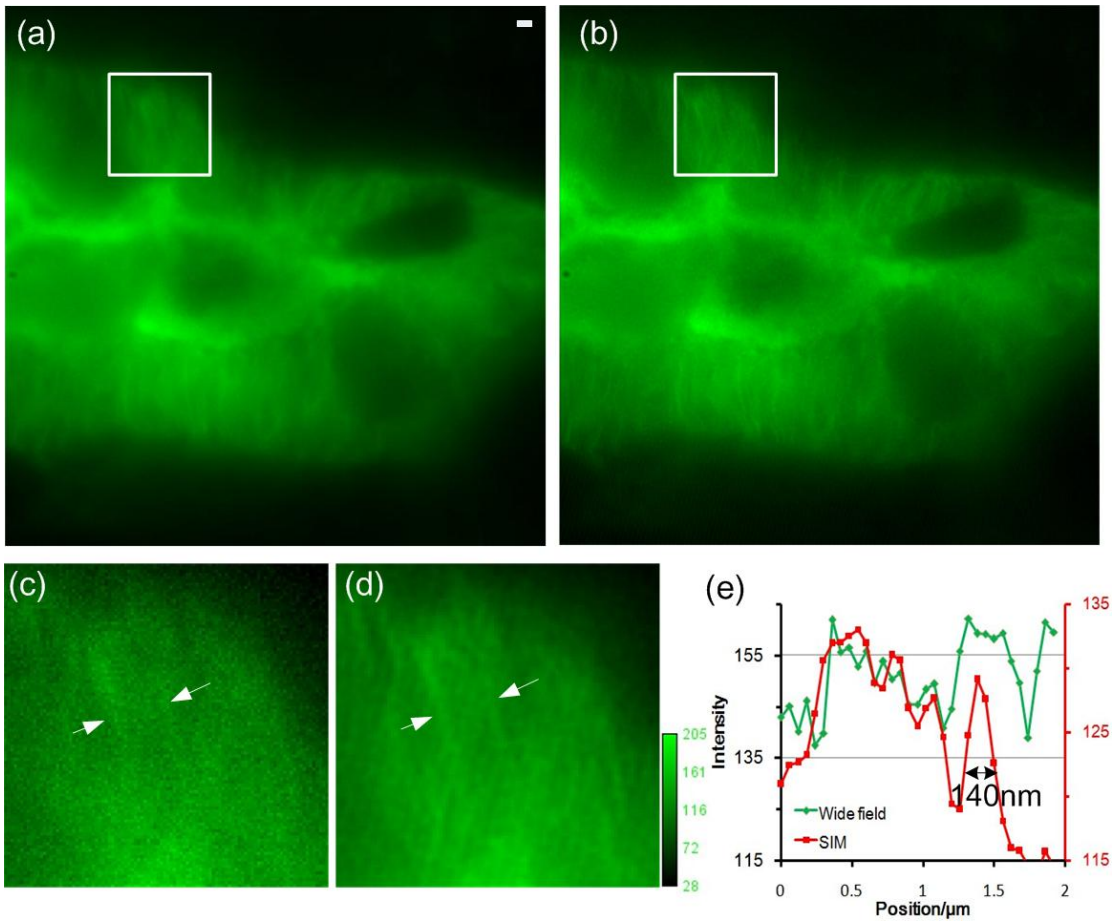

Supplementary Figure 4 Comparison of the wide-field (a) and SIM imaging (b) at 488 nm excitation for the fine structure of the convoluted tubule in the mouse kidney. Magnifications of the boxed areas (yellow) in (a), (b) were shown in (c) and (d), respectively. The intensity along the line in (c) and (d) are plotted in (e). Pixel sizes of the wide-field and SIM microscopy are 60 nm, and the exposure time is 9 s for each frame. Scale bar, 1 μm.

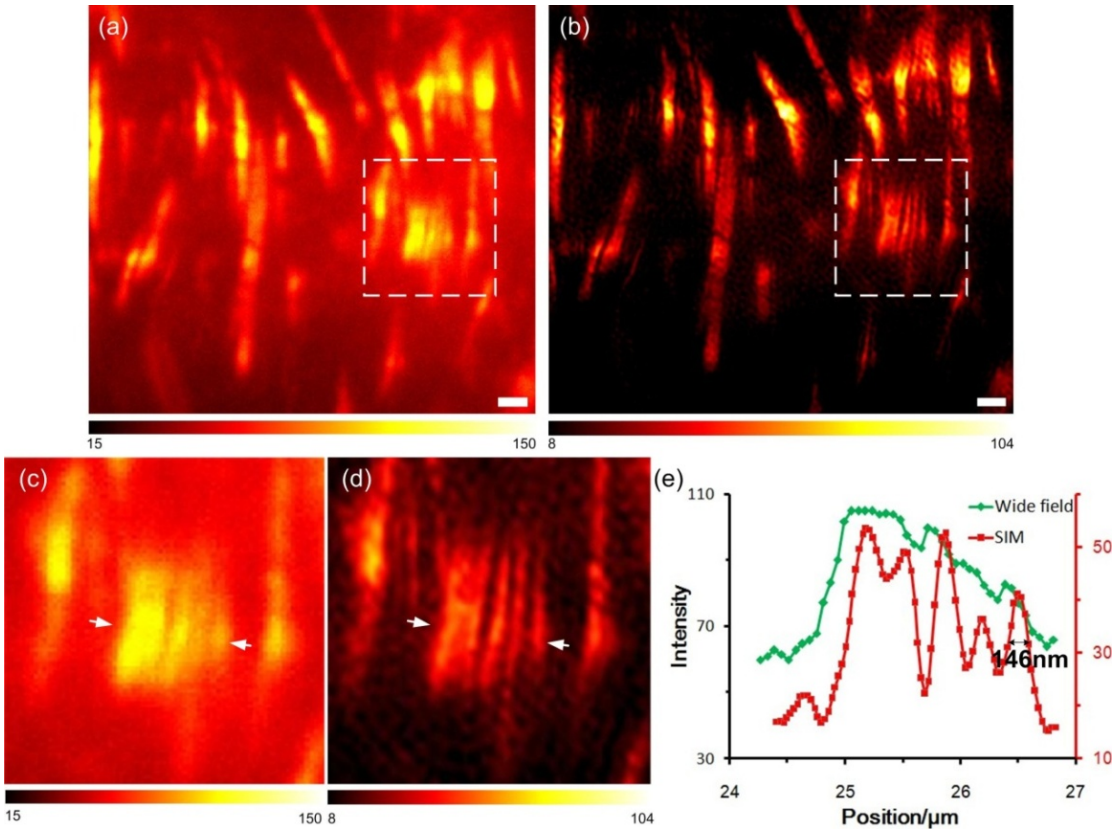

Supplementary Figure 5 Comparison of the wide-field (a) and SIM imaging (b) at 561 nm excitation for the brush boarder of the mouse kidney. Magnifications of the boxed areas (yellow) in (a), (b) were shown in (c) and (d), respectively. The intensity along the line in (c) and (d) are plotted in (e). Pixel sizes of the wide-field and SIM microscopy are 60 nm and 30 nm, respectively, and the exposure time is 9 s for each frame. Scale bar, 1 μm.